Journal of CO2 Utilization 50 (2021) 101609

Contents lists available at ScienceDirect

Journal of CO2 Utilization

journal homepage: www.elsevier.com/locate/jcou

CO_2 hydrogenation to methanol over partially embedded Cu within Zn-Al oxide and the effect of indium

Kristian Stangeland [a], Fawzi Chamssine [a], Wenzhao Fu [b], Zikun Huang [b], Xuezhi Duan [b,*], Zhixin Yu [a,*]

[a] Department of Energy and Petroleum Engineering, University of Stavanger, 4036 Stavanger, Norway
[b] State Key Laboratory of Chemical Engineering, East China University of Science and Technology, 200237 Shanghai, China

ARTICLE INFO

Keywords:
CO_2 hydrogenation
Methanol
Copper
Zinc
Indium
Hydrotalcite

ABSTRACT

Developing effective catalysts for CO_2 hydrogenation to methanol is an important step to improve the efficiency of a promising process for green synthesis of fuels and chemicals. Optimizing the Cu dispersion is often the main goal in preparing Cu/ZnO-based catalysts due to the strong dependence of the catalytic activity on the Cu surface area. However, the catalytic properties are also related to the nature of the Cu-ZnO interface. Herein, a series of hydrotalcite-derived $Cu/ZnO/Al_2O_3$ catalysts were prepared for CO_2 hydrogenation to methanol. The preparation method results in partially embedded Cu particles within the Zn-Al oxide matrix. This microstructure exhibits significantly enhanced intrinsic activity and methanol selectivity. Loss of the interfacial area between Cu and Zn-Al mixed oxide phase due to sintering of Zn-Al matrix is identified as the main reason for deactivation of the HT-derived catalysts. The influence of In on Cu/ZnO-based catalysts is also investigated. It is found that In decreases the activity but increases the methanol selectivity and stabilizes the Cu particles and the Zn-Al mixed oxide phase. The lower activity of the In-containing catalysts is linked to the inhibition of Cu active sites by Cu_xIn_y species.

1. Introduction

The increasing atmospheric CO_2 concentration has led to extensive efforts to develop environmental-friendly solutions for high-emission sectors. CO_2 hydrogenation to methanol is one of the most promising methods for producing fuels and chemicals from renewable sources [1]. This is because methanol synthesis from syngas (CO, CO_2, H_2) is already a well-established process. Furthermore, methanol is an important feedstock for several processes in the chemical industry, such as chloromethane, acetic acid, methyl tert-butyl ether (MTBE), alkyl halides, and formaldehyde [2–4]. As such, the infrastructure is already in place to handle methanol or methanol-derived fuels as primary energy carriers. One of the main issues is the current high price of hydrogen produced from renewable sources [5]. However, the price of renewable hydrogen is expected to decrease in the future, which can improve the economic viability of the CO_2-to-methanol process.

Methanol synthesis from CO_2 (Eq. (1)) is exothermic and a volume-reducing reaction. The main side reaction is the reverse water-gas shift (RWGS) reaction (Eq. (2)), which converts CO_2 into CO and becomes more favorable at higher temperatures. Hence, low temperature (200–300 °C) and moderate pressure (50–100 bar) are typically employed in CO_2 hydrogenation to methanol [6,7].

$$CO_2 + 3H_2 \rightleftarrows CH_3OH + H_2O \quad \Delta H = -49.5\ kJ/mol \tag{1}$$

$$CO_2 + H_2 \rightleftarrows CO + H_2O \quad \Delta H = 41.2\ kJ/mol \tag{2}$$

The $Cu/ZnO/Al_2O_3$ system has been studied for decades. The industrial $Cu/ZnO/Al_2O_3$ catalyst consists of an intimate mixture of Cu and metal oxide nanoparticles, typically obtained from co-precipitation of metal nitrates and forming a Cu, Zn carbonate precursor [8]. This synthesis route usually results in a high Cu surface area and highly active catalysts. Besides the Cu dispersion, the activity of Cu/ZnO-based catalysts has also been linked to synergetic effects between Cu and ZnO, which is often referred to as the strong metal-support interaction (SMSI). Several models of the Cu-ZnO synergy in Cu-based catalysts have been proposed. Experimental and computational studies have identified Cu lattice strain or defects as indicative of high performance, which might also be influenced by the properties of the metal oxide phase [4,9,10].

* Corresponding authors.
E-mail addresses: xzduan@ecust.edu.cn (X. Duan), Zhixin.yu@uis.no (Z. Yu).

https://doi.org/10.1016/j.jcou.2021.101609
Received 18 March 2021; Received in revised form 2 June 2021; Accepted 4 June 2021
Available online 12 June 2021

There is also compelling evidence that the SMSI between Cu and ZnO is crucially involved in the active sites of methanol synthesis [4,11–14]. Studt et al. [12] showed that a relatively inactive Cu/MgO catalyst can be converted into an efficient CO_2-to-methanol catalyst by impregnating ZnO onto Cu/MgO. The SMSI has been ascribed to the formation of CuZn [4,15] or $CuZnO_x$ [16] surface alloy species. This is supported by a correlation between the Zn coverage of Cu and the methanol synthesis activity, which has been demonstrated for conventional catalysts [17] and model structures [15,18]. Furthermore, oxygen vacancies in the ZnO at the Cu-ZnO interface might assist in CO_2 activation and conversion to methanol [19]. The optimization of Cu dispersion can be regarded as highly advanced for this system. However, higher intrinsic activity, i.e., normalized to the Cu surface area, has been reported for partially embedded Cu nanoparticles into a mixed Zn-Al oxide matrix [20,21]. Therefore, tuning the microstructural properties and the Cu-metal oxide interface are key areas for enhancing the activity of Cu/ZnO-based catalysts.

Recently, In_2O_3-based catalysts, typically promoted by metal oxides (e.g., Zr [22], Y [23], La [23]) or Pd [24–26] have received significant interest due to their high methanol selectivity and stability over a wide range of reaction temperatures (200–320 °C). Only a limited number of studies have investigated In incorporation into Cu-based catalysts [27–34]. Matsumura et al. [27] found that the addition of In_2O_3 reduces the activity but enhances the stability and suppresses the formation of CO in high-temperature methanol steam reforming over Cu/ZnO-based catalysts. Similar effects of In_2O_3 have also been reported in CO_2 hydrogenation to methanol [30,34]. On the other hand, Shi et al. [32] obtained active and selective Cu-In_2O_3 catalysts prepared by co-precipitation for CO_2 hydrogenation to methanol. The most active catalyst consisted of Cu_9In_{11} alloy in intimate contact with an In_2O_3 phase. They proposed that a synergistic effect is present for $Cu_{11}In_9$-In_2O_3 catalyst in which H_2 is dissociatively adsorbed on the $Cu_{11}In_9$ surface and CO_2 is activated at In_2O_3 oxygen vacancies. These species subsequently migrate to the interfacial sites where CO_2 is hydrogenated to methanol. Gao et al. [31] found that the activity and selectivity of Cu-In_2O_3-ZrO_2 catalyst containing Cu_2In alloy are higher than In_2O_3 and In_2O_3-ZrO_2 catalysts. These contradictory findings highlight that different Cu-In speciation and their effects on CO_2 hydrogenation to methanol are not fully understood. Furthermore, the cause of the highly inhibiting effect of small amounts of In_2O_3 on the activity of Cu/ZnO catalysts has not been identified.

Herein, we report a facile strategy for the synthesis of active Cu/ZnO-based catalysts for CO_2 hydrogenation to methanol. Partially embedding Cu within a Zn-Al oxide matrix is obtained via a hydrotalcite (HT)-like precursor and compared to a coprecipitated Cu/ZnO catalyst. We show that enhancing the Cu-metal oxide interfacial contact can be utilized to develop more active Cu/ZnO-based catalysts. Furthermore, the influence of In on Cu/ZnO-based catalysts is also elucidated, where the incorporation of In can stabilize the Cu-metal oxide interface but reduces the catalyst activity. Anchoring In within the Zn-Al oxide phase seems to be the key to avoid the negative effects of In on the activity. The present findings provide a promising approach for optimizing the Cu-metal oxide interaction, which can further enhance the catalytic performance of Cu-based catalysts for CO_2 hydrogenation to methanol.

2. Experimental

2.1. Catalyst preparation

The HT-like catalyst precursors containing Cu, Zn, Al, and In were prepared by co-precipitation at room temperature. For a typical synthesis, a 200 mL aqueous solution of metal salts ($Cu(NO_3)_2 \cdot 3H_2O$, $Zn(NO_3)_2 \cdot 6H_2O$, $Al(NO_3)_3 \cdot 9H_2O$, and $In(NO_3)_3 \cdot H_2O$) with a metal concentration of 0.5 M was added dropwise into a 200 mL mixed solution of NaOH (0.2 mol) and Na_2CO_3 (0.025 mol) precipitant under vigorous stirring. The pH of the precipitate solution after mixing was adjusted to 9.0 ± 0.2 if needed. The precursor solution was aged at 60 °C for 15 h before the precipitate was filtered and washed with deionized water. Finally, the product was dried overnight at 80 °C and then calcined in flowing synthetic air at 500 °C for 4 h. The HT-derived catalysts with a Cu:Zn ratio of 2 are denoted as 2CuZnAl-In*Y*, where *Y* refers to the mol% of In (*Y* = 0–5 mol%). Table 1 lists the nominal and the actual metal content determined from ICP-AES of the 2CuZnAl-In*Y* catalysts.

We also prepared a binary Cu-ZnO by co-precipitation following a procedure described by Behrens and Schlögl [8]. In brief, an aqueous Cu and Zn nitrate solution with metal concentration of 1 M (Cu:Zn = 5:1) was co-precipitated at a constant pH of 6.5 using a 1.2 M sodium carbonate solution as precipitating agent. The co-precipitate was aged in the mother liquor at 60 °C for 15 h. The precipitate was washed several times with deionized water, dried, and then the precursors were calcined in flowing air at 350 °C for 4 h. The ternary In/Cu-ZnO catalyst was obtained by impregnating Cu/ZnO with In nitrate. The impregnated catalyst was calcined again at 350 °C for 4 h. The composition of the Cu-ZnO and In/Cu-ZnO catalysts is also given in Table 1.

2.2. Catalyst characterization

The specific surface area and pore size distribution of the catalysts were determined from N_2 adsorption-desorption at 77 K by the Brunauer-Emmet-Teller (BET) and Barret-Joyner-Halenda (BJH) methods, respectively. The measurements were conducted using a Micromeritics TriStar II instrument. Degassing of the samples prior to analysis was done at 120 °C for 14 h with a Micromeritics VacPrep 061 degas system.

Elemental analysis of the catalysts was performed by ICP-AES on an Agilent 725-ES apparatus. Typically, 200 mg of sample was dissolved in a HNO_3:HCl mixture with a ratio of 1:3 at elevated temperature until complete dissolution of the catalyst. The sample was further diluted and filtered prior to elemental analysis.

The high-angle annular dark-field scanning transmission microscopy (HAADF-STEM) images were collected on a Tecnai G2F20 S-Twin instrument operated at 200 kV. The reduced and passivated catalysts were dispersed in ethanol by ultrasonication, then one drop of the solution was deposited on a holey carbon-coated support grid.

X-ray diffraction (XRD) patterns were recorded on either a Rigaku D/Max 2550 VB/PC or Bruker-AXS Microdiffractometer (D8 ADVANCE) instrument using a Cu Kα radiation source (λ = 1.5406, 40 kV, and 40 mA). The patterns were typically obtained at 2θ between 10–90° with a step interval of 2°/min. The peaks were indexed according to the Joint Committee on Powder Diffraction Standards (JCPDS) database.

X-ray photoelectron spectroscopy (XPS) and Auger (XAES) spectra were recorded on a ThermoFisher ESCALAB250Xi equipped with a monochromatic Al K_α source (1486.6 eV) operated at 15 kV. High-resolution spectra were obtained at a pass energy of 30.0 eV, step size of 0.05 eV, and dwell time of 500 ms per step. All spectra were referenced to the C 1s peak (284.8 eV).

Temperature programmed reduction (H_2-TPR) profiles were recorded using a Micromeritics Autochem II ASAP 2920 instrument. Prior to

Table 1
Nominal and actual catalyst compositions determined from ICP-AES of the 2CuZnAl-In*Y* catalysts.

Catalysts	Nominal metal content (mol%)				Metal content determined by ICP-AES (mol%)			
	Cu	Zn	Al	In	Cu	Zn	Al	In
2CuZnAl-In0	50	25	25	0	51.3	24.3	24.4	–
2CuZnAl-In2	50	25	23	2	50.9	24.1	22.9	2.1
2CuZnAl-In3	50	25	22	3	51.5	24.6	20.8	3.1
2CuZnAl-In5	50	25	20	5	51.7	23.9	19.3	5.1
Cu-ZnO	83	17	–	–	83.2	16.8	–	–
In/Cu-ZnO	82	17	–	1	82.2	16.5	–	1.3

the measurements, the samples were pretreated at 200 °C in He flow for 30 min. The profiles were recorded by passing a 7% H_2/Ar mixture at 50 mL/min over the sample while the temperature was ramped from ambient to 500 °C at 10 °C/min.

The Cu surface area (SA_{Cu}) was determined by dissociative N_2O adsorption [35] using a Micromeritics Autochem 2920 instrument. The sample was first pretreated in He at 120 °C for 1 h followed by reduction in 7% H_2/Ar mixture (50 mL/min) for 2 h at 350 °C. Then, the catalyst bed was purged with He until the temperature reached 50 °C. The oxidation of surface Cu atoms to Cu_2O by N_2O adsorptive decomposition was carried out in a flow of 1% N_2O/He at 50 °C for 1 h. After that, the sample tube was purged with He for 1 h to remove the unreacted N_2O. Finally, the H_2 consumption of surface Cu_2O was measured by a second TPR experiment from 50 to 400 °C at a rate of 10 °C/min in a 7% H_2/Ar mixture.

2.3. Catalytic activity tests

The catalysts were tested for CO_2 hydrogenation to methanol in a custom-built fixed-bed continuous-flow reactor. Typically, 0.2 g of catalyst was mixed with SiC (2 g) and placed in a stainless tube reactor with an internal diameter of 0.5 cm and a length of 50 cm. The catalysts were reduced at 350 °C with a heating rate of 2 °C/min by 10% H_2/N_2 (50 mL/min). Finally, the reactor was cooled to ambient temperature, pressurized with the reactant gases ($H_2/CO_2/N_2$ = 3/1/1), and then heated to the desired reaction temperature. The post-reactor lines and valves were heated to 140 °C to avoid product condensation. An Agilent 7890 B gas chromatogram (GC) system fitted with two TCD detectors was used for on-line analysis of the products. The CO_2 conversion, methanol selectivity, and space-time yield (STY) of methanol were calculated by utilizing N_2 as internal standard. The TOF was calculated as the number of methanol molecules produced per surface Cu atom of the reduced catalyst per second. A CO_2 conversion of approximately 5% was used for the TOF measurements to exclude the effect of water inhibition.

3. Results and discussion

3.1. Catalyst characterization

3.1.1. Textural and structural properties of the 2CuZnAl-InY catalysts

The N_2 adsorption-desorption isotherms of the calcined catalysts are shown in Fig. S1. The BET surface area (SA_{BET}), pore volume, and average pore diameter of the calcined catalysts are summarized in Table 2. It can be seen that the incorporation of In slightly increases the BET surface area of the 2CuZnAl-In*Y* catalysts, which is in the range of 36–41 m^2/g. Furthermore, the pore volume is also higher for the In-containing catalysts (0.08–0.09 cm^3/g) compared to the 2CuZnAl-In0 catalyst (0.06 cm^3/g).

Table 2
Summary of N_2-physisorption, crystallite size, and average particle size of the 2CuZnAl-In*Y* catalysts.

Catalyst	SA_{BET} (m^2/g)	Pore volume (cm^3/g)	Average pore diameter (nm)	d_{Cu} (nm)[a]	d_{Cu} (nm)[b]
2CuZnAl-In0	36	0.06	6.2	13.1	9.5
2CuZnAl-In2	39	0.09	6.7	11.8	9.4
2CuZnAl-In3	41	0.09	6.7	12.1	9.4
2CuZnAl-In5	37	0.08	6.6	12.3	8.7
Cu-ZnO	72	0.17	7.7	23.7	–
In/Cu-ZnO	46	0.11	7.6	20.1	–

[a] Calculated from the Cu(111) peak by the Scherrer equation.

[b] Determined by counting particles in HAADF-STEM images.

The XRD patterns of the HT precursors are shown in Fig. 1a. The patterns are typical for HT-like structures such as $Cu_2Zn_4Al_2(OH)_{16}CO_3 \cdot H_2O$ (PDF 38-0484) [21]. The peaks at 2θ of 35.5° and 38.7° are attributed to CuO (PDF #48-1548). Crystalline CuO can be formed by the oxolation reaction, which transforms $Cu(OH)_2$ into CuO. The oxolation reaction can occur at relatively low temperatures for $Cu(OH)_2$ at high pH and can also take place during the drying process [36]. At high In content, additional reflections corresponding to $In(OH)_3$ (PDF #76-1463) are present at ~22.3° and ~31.7° for the 2CuZnAl-In5 catalyst. The full width at half maximum (FWHM) of the 003 reflection at 2θ of ~11.8° is related to lattice strain or crystal domain size in the stacking direction. As shown in Fig. 1b, a volcano-type trend with respect to In content can be observed. The volcano-trend in the FWHM of the 003 reflection indicates that a small fraction of In is incorporated into the HT-like structure [37–39]. The XRD pattern of the Cu-ZnO precursor is shown in the Supporting Information (Fig. S2a) and is typical of Cu, Zn malachite [40].

The calcined 2CuZnAl-In*Y* samples show weak reflections corresponding to CuO, whereas Zn or Al species cannot be identified (Fig. S3). The XRD patterns of the reduced-passivated 2CuZnAl-In*Y* catalysts are shown in Fig. 2a. The reflections at 2θ of 43.3°, 50.4, and 74.1° correspond to metallic Cu (PDF #04-0836). The crystallite size of Cu was estimated from the Cu(111) peak, and the crystallite size is relatively similar for the 2CuZnAl-In*Y* catalysts between 11.8–13.1 nm (Table 2). The weak reflection at 2θ of 36.3° is attributed to ZnO (PDF #36-1415) and indicates that the Zn-Al species are highly dispersed, which is typical for HT-derived CuZnAl catalysts [21,41]. The regions of the Cu peaks are magnified in Fig. 2b. A shift in the Cu peaks towards lower diffraction angles is observed with increasing In content. Furthermore, weak reflections are present between 42–43° for the 2CuZnAl-In5 catalyst. This is attributed to the formation of Cu_xIn_y alloy because the most intense peaks of different Cu_xIn_y alloys are located in this region. Moreover, it has been demonstrated that Cu_xIn_y alloys can form under the reduction conditions used in this work [32,42,43]. Crystalline Cu and ZnO phases can be identified for the Cu-ZnO and In/Cu-ZnO catalysts (Fig. S2b). The crystallite size of Cu-ZnO (23.7 nm) is slightly larger than that of the In/Cu-ZnO catalyst (Table 2).

HAADF-STEM was used to investigate the microstructure of the 2CuZnAl-In*Y* catalysts. The calcined catalysts consist of a largely amorphous mixed oxide phase, as depicted in Fig. 3a for the 2CuZnAl-In0 catalyst. This is typical for HT precursors, which are composed of a highly dispersed mixed metal oxide phase after calcination [36]. As illustrated in Fig. 3b, larger Cu particles are formed for the 2CuZnAl-In*Y* catalyst after reduction, which are embedded within a metal oxide matrix. In literature, the metal oxide matrix is reported to contain a spinel-like $ZnAl_2O_4$ structure [21,36]. The structure of the other reduced In-containing 2CuZnAl-In*Y* catalysts is similar (Fig. S4a–c). The structure of the 2CuZnAl-In*Y* catalysts is obviously different from the conventionally prepared Cu/ZnO catalysts, which is characterized by crystalline CuO particles dispersed by discrete ZnO particles (Fig. 3c). The continuous embedding metal oxide matrix for the 2CuZnAl-In*Y* catalysts probably leads to a larger Cu-metal oxide interface compared to the Cu/ZnO catalyst. The average Cu particle size of the 2CuZnAl-In*Y* catalysts was determined by measuring at least 400 particles and are summarized in Table 2. The particle size distribution is shown in Fig. S5a–d. The average Cu particle size is comparable for the 2CuZnAl-In*Y* catalysts (8.7–9.5 nm), which is smaller than the crystallite size estimated by XRD. This is probably because XRD is a volume-averaged technique and is more sensitive to larger crystallites [14].

3.1.2. XPS study of the 2CuZnAl-InY catalysts

The surface composition of the 2CuZnAl-In*Y* catalysts before and after reduction is summarized in Table 3. It can be seen that the surface

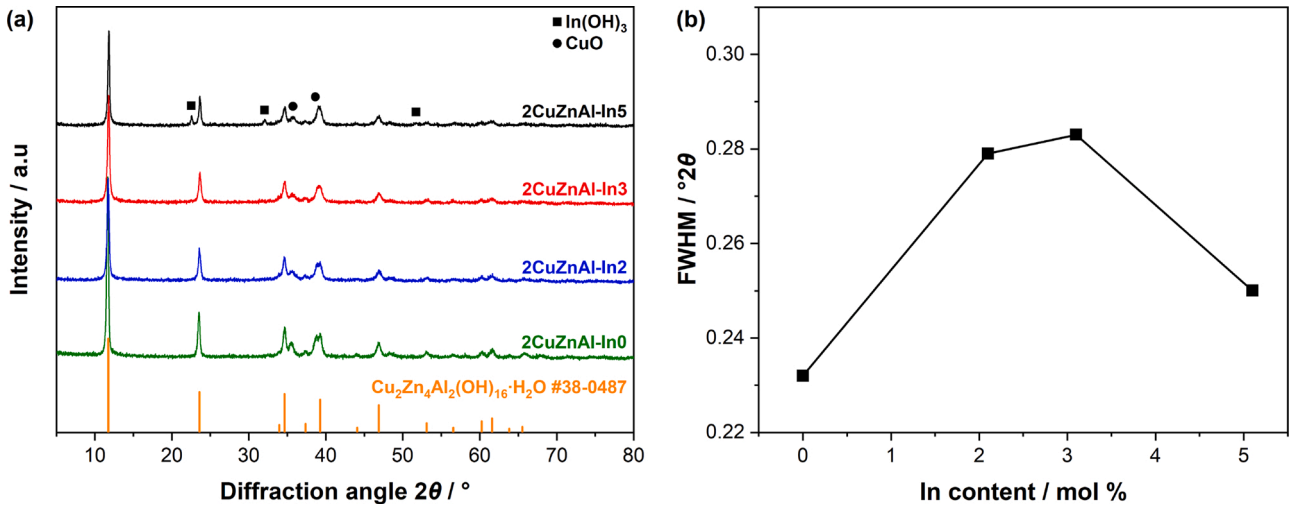

Fig. 1. (a) XRD patterns of the 2CuZnAl-In*Y* precursors and (b) FWHM of the 003 peak as a function of In content.

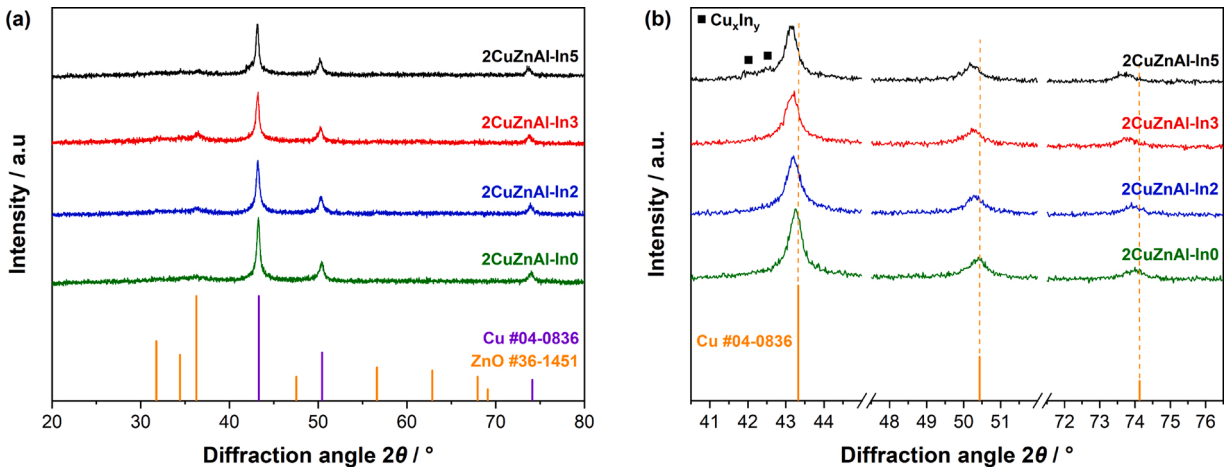

Fig. 2. (a) XRD patterns of the reduced-passivated 2CuZnAl-In*Y* catalysts and (b) the region containing the Cu diffraction peaks.

composition of the 2CuZnAl-In*Y* catalysts deviates from the nominal composition. The Cu:Zn ratio on the surface is close to 1.2 for the calcined samples, whereas the Cu:Zn ratio determined from ICP-AES is around 2. This is probably because the CuO species are embedded in the mixed metal oxide matrix after calcination, leading to a higher surface concentration of Zn and Al. In agreement with previous studies [4,30,44], the Cu/Zn surface ratio further decreases to ~0.9–0.6 after reduction, where the surface Zn concentration increases with increasing In content.

Fig. 4a shows the Cu $2p_{3/2}$ spectra of the calcined and reduced 2CuZnAl-In*Y* catalysts. The calcined samples exhibit a principal peak at ~934 eV and a characteristic satellite feature around 940–944 eV [45]. The satellite feature disappears after reduction, indicating that CuO species are not present after reduction. Furthermore, the main peak shifts towards lower binding energy, which is in the region of Cu° (932.6 eV) and Cu_2O (932.4 eV). The Cu L_3VV Auger line was investigated to obtain further information about the chemical state of Cu in the catalysts after reduction. For the calcined samples, a peak at 917.7 eV is detected (Fig. S6), which is close to the expected peak position of CuO [46]. The CuL_3VV Auger spectra of the reduced and passivated catalysts are shown in Fig. 4b. Since CuO species are not present after reduction in the Cu2p spectra, the profiles are deconvoluted into Cu° (~918.5 eV) eV) and Cu^+ (~916.4 eV). This estimation is widely used to determine the relative amount of Cu° and Cu^+ species in the sample [47–51]. It is clear that the majority of the Cu species exist as Cu^+ for all the catalysts, indicating high interaction between Cu and the metal oxide phase [47,48]. The Cu° fraction of the 2CuZnAl-In*Y* catalysts increases with increasing In content (Table 3).

To address the chemical state of Zn, the Zn $L_3M_{4,5}M_{4,5}$ Auger line was recorded. The Zn $L_3M_{4,5}M_{4,5}$ spectra of calcined and reduced 2CuZnAl-In*Y* are shown in Fig. 5a. It can be seen that the spectra of the calcined and reduced sample overlap, indicating that the chemical state of ZnO is largely unchanged after reduction. The chemical state of In was also examined, and the In 3d spectra contain two peaks at 444.8 eV and 452.3 eV corresponding to the In $3d_{5/2}$ and In $3d_{3/2}$ spin-orbit doublets (Fig. 5b) [52]. The peaks shift slightly towards lower binding energy after reduction. It is likely that the shift in the In 3d spectra is related to the formation of Cu_xIn_y alloys, in agreement with the XRD observations. The slight shift in the In 3d spectra indicate that a mix of In_2O_3 and Cu_xIn_y species are present after reduction [32,43,53].

3.1.3. *Reducibility of the catalysts*

H_2-TPR was carried out to investigate the reducibility of the catalysts. The TPR profiles of the 2CuZnAl-In*Y* catalysts are shown in Fig. 6a. The reduction of the 2CuZnAl-In*Y* catalysts occurs over a wide temperature range, and the profiles are deconvoluted into four peaks, namely α, β, γ_1, and γ_2. The low-temperature peaks are assigned to CuO particles dispersed on the catalyst's surface (α) and CuO particles in the bulk of the Zn-Al oxide (β) [47,54]. Additional high-temperature peaks are only observed for the HT-derived catalysts. The γ_1 and γ_2 peaks

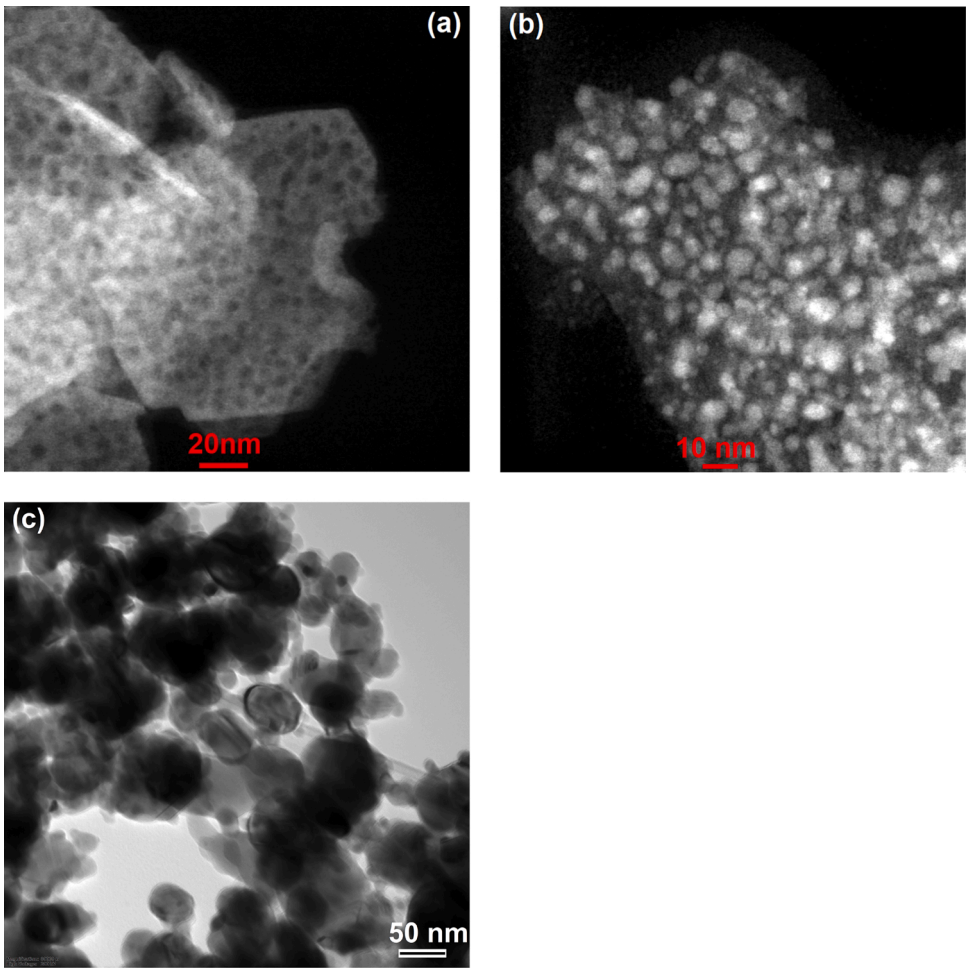

Fig. 3. HAADF-STEM images of the (a) calcined and (b) reduced 2CuZnAl-In0 catalyst; (c) TEM image of the reduced Cu-ZnO catalyst.

Table 3
Surface composition of calcined and reduced 2CuZnAl-In*Y* catalysts determined by XPS.

Catalyst	Surface composition after calcination (atom%)				Surface composition after reduction (atom %)				Cu^0 / (Cu^+ + Cu^0)
	Cu	Zn	Al	In	Cu	Zn	Al	In	
2CuZnAl-In0	37	31	32	0	33	36	30	0	0.15
2CuZnAl-In2	38	31	28	3	32	37	28	3	0.17
2CuZnAl-In3	38	32	25	5	30	40	25	5	0.22
2CuZnAl-In5	39	33	22	6	27	42	24	7	0.21

located between 250–300 °C are attributed to the reduction of Cu^{2+} species highly dispersed within the metal oxide matrix [9,21]. These Cu^{2+} species are strongly bound to the Zn-Al oxides, which results in a stabilization of the Cu_2O intermediate and a step-wise reduction of CuO (CuO → Cu_2O and Cu_2O → Cu) [55–57]. At moderate In content, the α and β peaks shift towards higher reduction temperature for 2CuZnAl-In*Y*. On the other hand, the γ peaks shift towards lower temperature with increasing In content. These observations indicate that moderate amounts of In enhance the interaction of CuO with the metal-oxide phase, whereas the Cu^{2+} species present in the metal oxide matrix are more easily reduced when the In content increases. In contrast, the complete reduction of the CuO particles of the Cu/ZnO and In/Cu-ZnO catalysts occurs at lower temperatures due to the weaker interaction with the metal oxide phase (Fig. 6b).

The H_2/CuO ratio was calculated to assess the H_2 consumption relative to the Cu content (Table 4). The H_2/CuO ratio is close to 100% for all the catalysts, indicating the complete reduction of CuO. A slight increase in the H_2/CuO ratio is observed with increasing In content for the 2CuZnAl-In*Y* catalysts, which is ascribed to the formation of Cu_xIn_y alloys. Similarly, the H_2/CuO ratio is higher when In is impregnated onto the Cu-ZnO catalyst.

3.1.4. N_2O titration measurements

The Cu surface area was estimated by N_2O dissociative adsorption. The Cu surface area of 2CuZnAl-In*Y* first increases from 13 to 16 m^2/g with the addition of 2 mol% In and then decreases with increasing In content (Table 4). The Cu surface concentration obtained by XPS indicates that the number of Cu atoms on the surface decreases with increasing In content, which can explain the lower Cu surface area of the 2CuZnAl-In3 and 2CuZnAl-In5 catalysts. In addition, the extent of Cu-In surface alloy formation might also influence the Cu surface area, as evidenced by the drop in Cu surface area from 18 m^2/g to 14 m^2/g when In is impregnated onto the Cu-ZnO catalyst.

3.2. Catalytic activity tests

3.2.1. Influence of Cu-metal oxide interface and In on activity

To assess the influence of the Cu surface area on the catalytic activity of HT-derived catalysts, we also prepared the 1CuZnAl-In*Y* and 4CuZnAl-In*Y* series of catalysts with an In content of 0–7 mol%, where 1 and 4

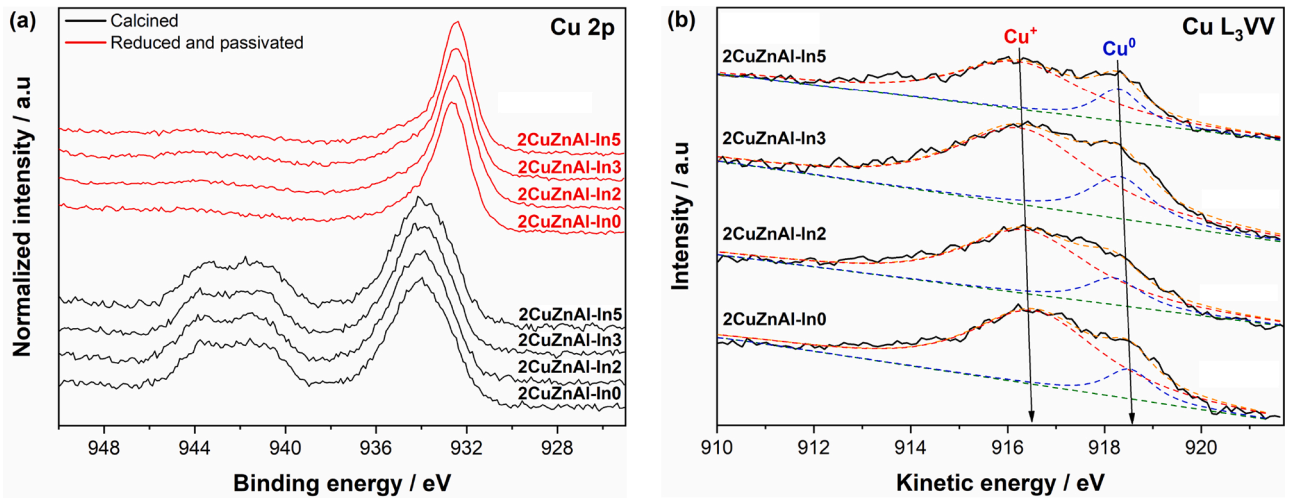

Fig. 4. (a) Cu $2p_{3/2}$ XPS spectra of the calcined and reduced 2CuZnAl-In*Y* catalysts. (b) Cu L_3VV Auger spectra of the reduced 2CuZnAl-In*Y* catalysts.

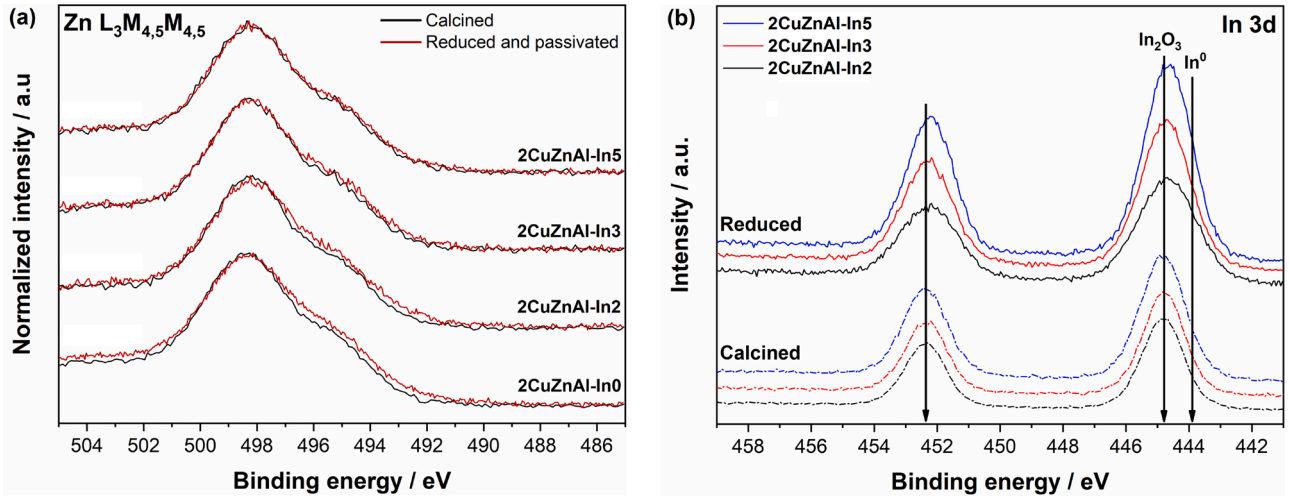

Fig. 5. (a) Zn $L_3M_{4,5}M_{4,5}$ Auger spectra of calcined and reduced 2CuZnAl-In*Y* catalysts. (b) In 3d XPS spectra of calcined and reduced 2CuZnAl-In*Y* catalysts.

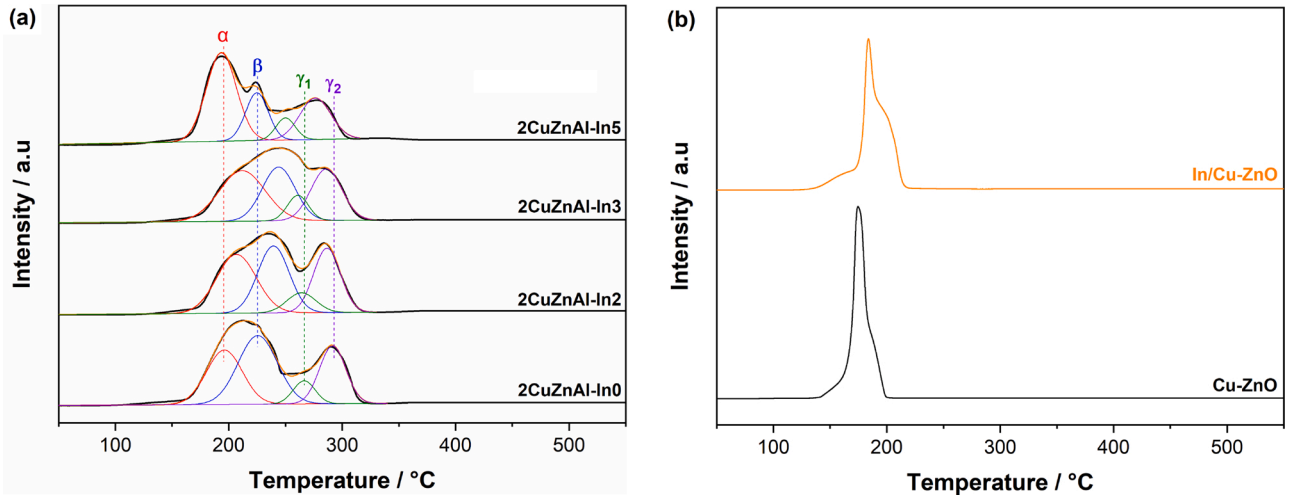

Fig. 6. (a) Deconvoluted H_2-TPR profiles of the 2CuZnAl-In*Y* catalysts and (b) H_2-TPR profiles of the Cu-ZnO and In/Cu-ZnO catalysts.

Table 4
Summary of the H_2-TPR data and the Cu surface area of the 2CuZnAl-In*Y* catalysts.

Catalyst	H_2/CuO (%)	TPR peak contribution (%)				SA_{Cu} (m^2/g_{cat})
		α	β	γ_1	γ_2	
2CuZnAl-In0	99	29	40	8	23	13
2CuZnAl-In2	101	34	32	8	26	16
2CuZnAl-In3	101	36	29	8	27	15
2CuZnAl-In5	103	48	20	9	23	11
Cu-ZnO	98	–	–	–	–	18
In/Cu-ZnO	101	–	–	–	–	14

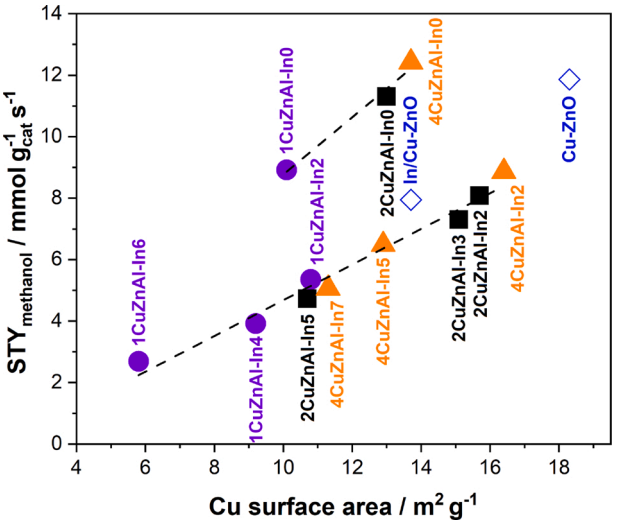

Fig. 7. STY of methanol as a function of Cu surface area of the CuZnAl-In*Y*, Cu-ZnO, and In/Cu-ZnO catalysts. Reaction conditions: 250 °C, 30 bar, $H_2/CO_2/N_2$ = 3/1/1, WHSV = 30 000 $cm^3\ g_{cat}^{-1}\ h^{-1}$.

refer to the Cu/Zn ratio. Table S1 summarizes the characterization results of the 1CuZnAl-In*Y* and 4CuZnAl-In*Y* catalysts. Fig. 7 shows the steady-state STY of methanol after 12 h testing plotted against the Cu surface area. It is evident that the methanol synthesis activity of the HT-derived catalysts is strongly correlated to the Cu surface area. This is often the case for Cu-based catalysts with a similar preparation history [58]. The highest STY of methanol (12.4 mmol $g_{cat}^{-1}\ h^{-1}$) is obtained over the 4CuZnAl-In0 catalyst, which also has the highest Cu surface area (14 m^2/g) of the HT-derived catalysts. The activity of the 4CuZnAl-In0 catalyst is higher than that of Cu/ZnO (11.9 mmol $g_{cat}^{-1}\ h^{-1}$), even though the 4CuZnAl-In0 catalyst has a lower Cu surface area. This is attributed to the larger number of interfacial sites due to the partial embedment of Cu in the Zn-Al matrix. The higher intrinsic activity of the HT-derived catalysts indicates that a compromise between high Cu surface area and Cu-metal oxide interfacial area is needed to maximize the activity of Cu/ZnO-based catalysts. The Zn-Al matrix obtained from HT-like precursor is a promising candidate for obtaining large Cu-metal oxide contact.

The activity of the In-containing HT-derived catalysts is also correlated to the Cu surface area, but is significantly lower compared to the In-free catalysts. Although the addition of 2 mol% In to HT-derived CuZnAl catalysts increases the Cu surface area, the STY of methanol is significantly reduced. The STY of methanol also decreases substantially when In is impregnated onto the Cu-ZnO catalyst. This suggests that In species covers or inhibits the active sites on the Cu surface. The lower activity of the In-doped catalysts is consistent with earlier studies [27,30,34].

To further assess the influence of the catalyst's composition, the turnover frequency (TOF) for methanol formation of the CuZnAl-In*Y*,

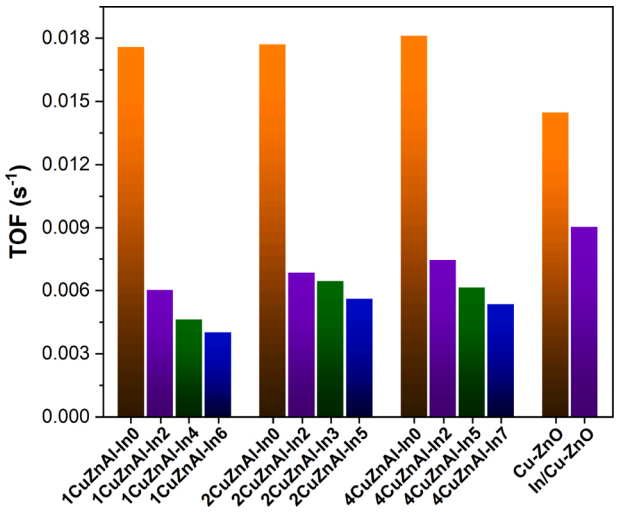

Fig. 8. TOF of methanol formation of the CuZnAl-In*Y*, Cu-ZnO, and In/Cu-ZnO catalysts. Reaction conditions: 250 °C, 30 bar, $H_2/CO_2/N_2$ = 3/1/1, CO_2 conversion ≈ 5%.

Cu-ZnO, and In/Cu-ZnO catalysts is compared in Fig. 8. The TOF of the CuZnAl-In0 catalysts is comparable at approximately 0.018 s^{-1}, which is higher than that obtained over the Cu/ZnO catalysts (0.014 s^{-1}). These TOFs are in the medium to high range compared with reported values in literature [21,58]. The vigorous debate regarding the Cu-ZnO synergy highlights the difficulty in identifying the dominant promotional mechanism in Cu/ZnO-based systems. Thus, the enhanced Cu-metal oxide interaction of the HT-derived catalysts might promote methanol synthesis by modifying the active Cu surface (e.g., inducing defects or promoting surface CuZn/$CuZnO_x$ formation [4,9,10]), providing a higher number of Cu-metal oxide interfacial sites [19], or a combination of these phenomena. It is interesting that the intrinsic activity of the CuZnAl-In0 catalysts is similar despite the differences in Cu particle size and composition. This further indicates that the enhanced Cu-metal oxide interaction is the main reason for the higher intrinsic activity of the HT-derived catalysts. When In is incorporated into the catalyst, the TOF decreases significantly. Furthermore, the TOF decreases with increasing In content for the HT-derived catalysts. Thus, In seems to have a dramatic effect on the ability of Cu to produce methanol. This is probably due to the presence of In species on the Cu surface or the formation of Cu_xIn_y alloy species, which seems to inhibit the activity of the Cu surface sites.

3.2.2. *Influence of Cu-metal oxide interface and In on methanol selectivity*

The methanol selectivity as a function of CO_2 conversion for the 2CuZnAl-In*Y*, Cu-ZnO, and In/Cu-ZnO catalysts is shown in Fig. 9. The 2CuZnAl-In0 catalyst exhibit higher methanol selectivity compared to the conventional Cu/ZnO catalyst. For Cu/ZnO-based catalysts, the Cu-ZnO interface or Cu-Zn surface alloy sites plays a crucial role in methanol synthesis [4,19,59]. Thus, the higher selectivity of 2CuZnAl-In0 compared to Cu-ZnO is ascribed to the superior interaction between Cu and the oxide matrix for the HT-derived catalyst. The methanol selectivity is also higher for the In-containing catalysts compared to the In-free catalysts. The maximum methanol selectivity is obtained at 3 mol % In. The higher selectivity of the In-containing 2CuZnAl-In*Y* catalysts is ascribed to the inhibition of CO formation. This is in agreement with Matsumura et al. [27], who observed that CO formation was suppressed by the presence of In on the Cu surface during methanol steam reforming over a Cu/ZnO-based catalyst.

3.2.3. *Stability of HT-derived catalysts and the deactivation mechanism*

The stability of the 2CuZnAl-In0 and 2CuZnAl-In3 catalysts was investigated over 72 h time on stream (TOS), and the CO_2 conversion

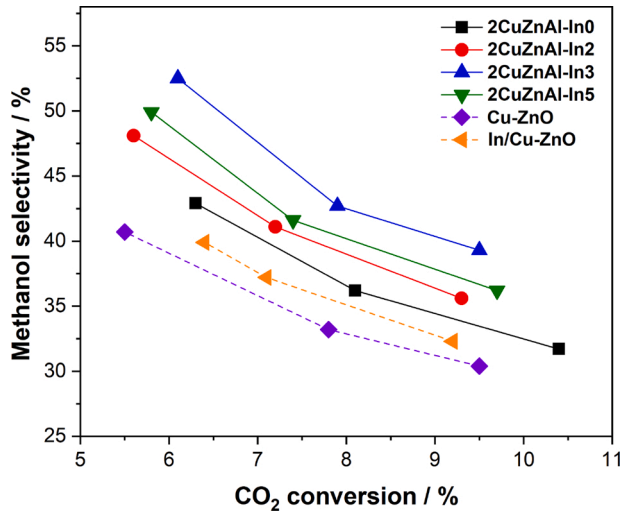

Fig. 9. Methanol selectivity at different CO_2 conversions for 2CuZnAl-In*Y*, Cu-ZnO and In/Cu-ZnO. The CO_2 conversion was varied by changing the contact time between 10 000 to 100 000 $cm^3/(g_{cat}$ h). Reaction conditions: 250 °C, 30 bar, $H_2/CO_2 = 3$.

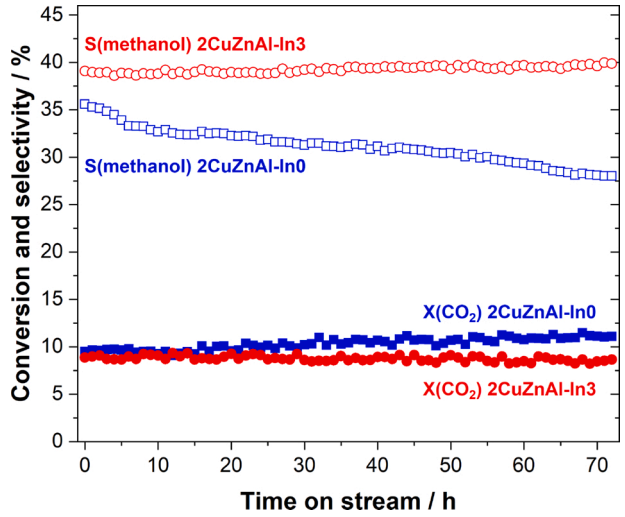

Fig. 10. CO_2 conversion and methanol selectivity over the 2CuZnAl-In0 and 2CuZnAl-In3 catalysts over 72 h TOS. Reaction conditions: 250 °C, 30 bar, $H_2/CO_2 = 3$.

and methanol selectivity are shown in Fig. 10. The CO_2 conversion and methanol selectivity remains relatively stable for the 2CuZnAl-In3 catalyst. A slight increase in CO_2 conversion is observed for the 2CuZnAl-In0 catalyst, whereas the methanol selectivity decreases from 35 to 28% (or 20%). Therefore, In could help to limit the deactivation of Cu-based catalysts during CO_2 hydrogenation to methanol if In can be stabilized in the Zn-Al oxide phase.

To gain further insight into the deactivation mechanism of the HT-derived catalysts, the spent catalysts were analyzed by N_2-physisorption, XRD, and N_2O chemisorption. Interestingly, the Cu surface area increases from 13 to 21 m^2/g for the 2CuZnAl-In0 catalyst after 72 h, whereas the Cu surface area is relatively unchanged for 2CuZnAl-In3 (Tables 5 vs. 4). Furthermore, the Cu particle size increased from 13 to 20 nm for the 2CuZnAl-In0 catalyst, while it only slightly increased from 12 to 14 nm for the 2CuZnAl-In3 catalyst (Tables 5 vs. 2). Therefore, the increase of Cu surface area for the 2CuZnAl-In0 catalyst is due to the structural changes of this catalyst. The XRD patterns of the spent catalysts are shown in Fig. 11. Crystalline $ZnAl_2O_4$ is observed for the spent 2CuZnAl-In0 catalyst, indicating that Zn-Al oxide matrix has sintered during the reaction. Therefore, the Zn-Al matrix appears to be more stable for the In-containing 2CuZnAl-In3 catalyst. This further demonstrates the importance of the Cu-metal oxide interface on the methanol synthesis activity of the HT-derived catalysts. The structural changes of the 2CuZnAl-In0 catalyst are probably also responsible for the increase in the BET surface area. Thus, it seems that In prevents the deactivation of the 2CuZnAl-In3 catalyst by stabilizing the interfacial sites responsible for methanol synthesis through stabilizing the Cu particles and the Zn-Al mixed oxide phase.

Table 5
Physicochemical properties of the spent 2CuZnAl-In0 and 2CuZnAl-In3 catalyst.

Catalyst	d_{Cu} (nm)[a]	SA_{BET} (m^2/g)	SA_{Cu} (m^2/g)
2CuZnAl-In0	20.3	74 (56)[b]	21
2CuZnAl-In3	14.5	58 (54)[b]	16

[a] Determined by XRD of the Cu(111) peak.

[b] BET surface area of the reduced-passivated catalysts.

4. Conclusion

In summary, partially embedded Cu particles into a Zn-Al oxide matrix were prepared via HT-like precursors. It was demonstrated that the intrinsic activity of the HT-derived catalysts is significantly higher than a Cu/ZnO catalyst. Thus, a higher space-time yield is achieved for the HT-derived catalyst despite having a smaller Cu surface area. Furthermore, the methanol selectivity is also higher for the HT-derived catalysts. The superior performance is attributed to the enhanced interaction between Cu and the Zn-Al oxide phase. The influence of In on the catalytic performance was also studied. Although the methanol selectivity is higher for the In-containing catalysts, the addition of In to Cu/ZnO-based catalysts reduces the activity. The lower activity of the In-containing catalysts is attributed to In inhibition of active sites on the Cu surface.

The importance of the Cu-metal oxide interaction is supported by the long-term stability tests. The intrinsic activity decreases substantially for the In-free catalyst. This is attributed to the reduced Cu-metal oxide interaction due to the sintering of Zn-Al oxide matrix. On the other hand, the incorporation of In stabilizes the Cu particles and Zn-Al mixed oxide phase, which limit the deactivation of the catalyst. The present study demonstrates the importance of the microstructure and Cu-metal oxide interface for CO_2 hydrogenation to methanol.

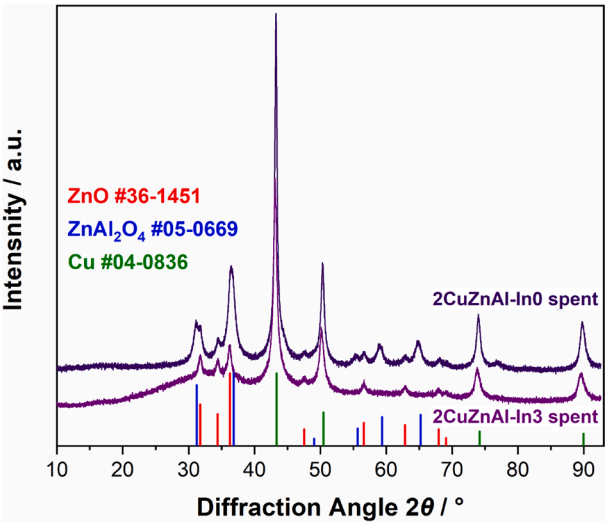

Fig. 11. XRD patterns of the spent 2CuZnAl-In0 and 2CuZnAl-In3 catalysts.

Author statement

Kristian Stangeland: Conceptualization, Investigation, Visualization, Writing – Original Draft **Fawzi Chamssine:** Investigation **Zikun Huang:** Investigation **Wenzhao Fu:** Investigation **Xuezhi Duan:** Conceptualization, Supervision, Writing – Review and Editing **Zhixin Yu:** Supervision, Writing – Review and Editing.

Declaration of Competing Interest

The authors of this manuscript certify that they have NO affiliations with or involvement in any organization or entity with any financial interest or non-financial interest in the subject matter or materials discussed in this manuscript.

Acknowledgements

The authors would like to thank the financial support from the Norwegian Ministry of Education and Research and the Department of Energy and Petroleum Engineering, University of Stavanger for this project.

Appendix A. Supplementary data

Supplementary material related to this article can be found, in the online version, at https://doi.org/10.1016/j.jcou.2021.101609.

References

[1] M. Aresta, A. Dibenedetto, E. Quaranta, State of the art and perspectives in catalytic processes for CO2 conversion into chemicals and fuels: the distinctive contribution of chemical catalysis and biotechnology, J. Catal. 343 (2016) 2–45.
[2] X.-M. Liu, G. Lu, Z.-F. Yan, J. Beltramini, Recent advances in catalysts for methanol synthesis via hydrogenation of CO and CO2, Ind. Eng. Chem. Res. 42 (2003) 6518–6530.
[3] G.A. Olah, Towards oil independence through renewable methanol chemistry, Angew. Chemie Int. Ed. 52 (2013) 104–107.
[4] M. Behrens, F. Studt, I. Kasatkin, S. Kühl, M. Hävecker, F. Abild-Pedersen, S. Zander, F. Girgsdies, P. Kurr, B.-L. Kniep, The active site of methanol synthesis over Cu/ZnO/Al2O3 industrial catalysts, Science 336 (2012) 893–897.
[5] Y. He, L. Zhu, J. Fan, L. Li, Comparative exergy and exergoeconomic analysis between liquid fuels production through chemical looping hydrogen generation and methane reforming with CO2, Energy Convers. Manage. 222 (2020), 113239.
[6] A. Álvarez, A. Bansode, A. Urakawa, A.V. Bavykina, T.A. Wezendonk, M. Makkee, J. Gascon, F.J.Cr. Kapteijn, Challenges in the greener production of formates/formic acid, methanol, and DME by heterogeneously catalyzed CO2 hydrogenation processes, Chem. Rev. 117 (2017) 9804–9838.
[7] K. Stangeland, H. Li, Z.J.I. Yu, E.C. Research, Thermodynamic analysis of chemical and phase equilibria in CO2 hydrogenation to methanol, dimethyl ether, and higher alcohols, Ind. Eng. Chem. Res. 57 (2018) 4081–4094.
[8] M. Behrens, R. Schlögl, How to prepare a good Cu/ZnO catalyst or the role of solid state chemistry for the synthesis of nanostructured catalysts, Zeitschrift für anorganische und allgemeine Chemie 639 (2013) 2683–2695.
[9] M.M. Günter, T. Ressler, B. Bems, C. Büscher, T. Genger, O. Hinrichsen, M. Muhler, R. Schlögl, Implication of the microstructure of binary Cu/ZnO catalysts for their catalytic activity in methanol synthesis, Catal. Lett. 71 (2001) 37–44.
[10] I. Kasatkin, P. Kurr, B. Kniep, A. Trunschke, R. Schlögl, Role of lattice strain and defects in copper particles on the activity of Cu/ZnO/Al2O3 catalysts for methanol synthesis, Angew. Chemie Int. Ed. 46 (2007) 7324–7327.
[11] K. Stangeland, H. Li, Z. Yu, CO2 hydrogenation to methanol: the structure–activity relationships of different catalyst systems, Energy Ecol. Environ. 5 (2020) 1–14.
[12] F. Studt, M. Behrens, E.L. Kunkes, N. Thomas, S. Zander, A. Tarasov, J. Schumann, E. Frei, J.B. Varley, F. Abild-Pedersen, The mechanism of CO and CO2 hydrogenation to methanol over Cu-based catalysts, ChemCatChem 7 (2015) 1105–1111.
[13] S. Tada, S. Kayamori, T. Honma, H. Kamei, A. Nariyuki, K. Kon, T. Toyao, K.-i. Shimizu, S. Satokawa, Design of interfacial sites between Cu and amorphous ZrO2 dedicated to CO2-to-methanol hydrogenation, ACS Catal. 8 (2018) 7809–7819.
[14] R. Van Den Berg, G. Prieto, G. Korpershoek, L.I. Van Der Wal, A.J. Van Bunningen, S. Lægsgaard-Jørgensen, P.E. De Jongh, K.P. De Jong, Structure sensitivity of Cu and CuZn catalysts relevant to industrial methanol synthesis, Nat. Commun. 7 (2016) 1–7.
[15] J. Nakamura, I. Nakamura, T. Uchijima, Y. Kanai, T. Watanabe, M. Saito, T. Fujitani, A surface science investigation of methanol synthesis over a Zn-deposited polycrystalline Cu surface, J. Catal. 160 (1996) 65–75.
[16] S. Kattel, P.J. Ramírez, J.G. Chen, J.A. Rodriguez, P. Liu, Active sites for CO2 hydrogenation to methanol on Cu/ZnO catalysts, Science 355 (2017) 1296–1299.
[17] S. Kuld, M. Thorhauge, H. Falsig, C.F. Elkjær, S. Helveg, I. Chorkendorff, J. Sehested, Quantifying the promotion of Cu catalysts by ZnO for methanol synthesis, Science 352 (2016) 969–974.
[18] S.D. Senanayake, P.J. Ramírez, I. Waluyo, S. Kundu, K. Mudiyanselage, Z. Liu, Z. Liu, S. Axnanda, D.J. Stacchiola, J. Evans, Hydrogenation of CO2 to methanol on CeO x/Cu (111) and ZnO/Cu (111) catalysts: role of the metal–oxide interface and importance of Ce3+ sites, J. Phys. Chem. C 120 (2016) 1778–1784.
[19] F. Liao, Y. Huang, J. Ge, W. Zheng, K. Tedsree, P. Collier, X. Hong, S.C. Tsang, Morphology-dependent interactions of ZnO with Cu nanoparticles at the materials' interface in selective hydrogenation of CO2 to CH3OH, Angew. Chemie 123 (2011) 2210–2213.
[20] M. Behrens, A. Furche, I. Kasatkin, A. Trunschke, W. Busser, M. Muhler, B. Kniep, R. Fischer, R. Schlögl, The potential of microstructural optimization in metal/oxide catalysts: higher intrinsic activity of copper by partial embedding of copper nanoparticles, ChemCatChem 2 (2010) 816–818.
[21] S. Kühl, A. Tarasov, S. Zander, I. Kasatkin, M. Behrens, Cu-based catalyst resulting from a Cu, Zn, Al hydrotalcite-like compound: a microstructural, thermoanalytical, and in situ XAS study, Chem. Eur. J. 20 (2014) 3782–3792.
[22] O. Martin, A.J. Martín, C. Mondelli, S. Mitchell, T.F. Segawa, R. Hauert, C. Drouilly, D. Curulla-Ferré, J. Pérez-Ramírez, Indium oxide as a superior catalyst for methanol synthesis by CO2 hydrogenation, Angew. Chemie Int. Ed. 55 (2016) 6261–6265.
[23] C.-Y. Chou, R.F. Lobo, Direct conversion of CO2 into methanol over promoted indium oxide-based catalysts, Appl. Catal. A: Gen. 583 (2019), 117144.
[24] N. Rui, Z. Wang, K. Sun, J. Ye, Q. Ge, C.-j. Liu, CO2 hydrogenation to methanol over Pd/In2O3: effects of Pd and oxygen vacancy, Appl. Catal. B: Environ. 218 (2017) 488–497.
[25] J.L. Snider, V. Streibel, M.A. Hubert, T.S. Choksi, E. Valle, D.C. Upham, J. Schumann, M.S. Duyar, A. Gallo, F. Abild-Pedersen, Revealing the synergy between oxide and alloy phases on the performance of bimetallic In–Pd catalysts for CO2 hydrogenation to methanol, ACS Catal. 9 (2019) 3399–3412.
[26] M.S. Frei, C. Mondelli, R. García-Muelas, K.S. Kley, B. Puértolas, N. López, O. V. Safonova, J.A. Stewart, D.C. Ferré, J. Pérez-Ramírez, Atomic-scale engineering of indium oxide promotion by palladium for methanol production via CO2 hydrogenation, Nat. Commun. 10 (2019) 1–11.
[27] Y. Matsumura, H. Ishibe, Durable copper–zinc catalysts modified with indium oxide in high temperature steam reforming of methanol for hydrogen production, J. Power Sources 209 (2012) 72–80.
[28] Y. Matsumura, Development of durable copper catalyst for hydrogen production by high temperature methanol steam reforming, Int. J. Hydrogen Energy 38 (2013) 13950–13960.
[29] Y. Matsumura, Durable Cu composite catalyst for hydrogen production by high temperature methanol steam reforming, J. Power Sources 272 (2014) 961–969.
[30] J. Słoczyński, R. Grabowski, P. Olszewski, A. Kozłowska, J. Stoch, M. Lachowska, J. Skrzypek, Effect of metal oxide additives on the activity and stability of Cu/ZnO/ZrO2 catalysts in the synthesis of methanol from CO2 and H2, Appl. Catal. A: Gen. 310 (2006) 127–137.
[31] J. Gao, F. Song, Y. Li, W. Cheng, H. Yuan, Q. Xu, Cu2In nanoalloy enhanced performance of Cu/ZrO2 catalysts for the CO2 hydrogenation to methanol, Ind. Eng. Chem. Res. 59 (2020) 12331–12337.
[32] Z. Shi, Q. Tan, C. Tian, Y. Pan, X. Sun, J. Zhang, D. Wu, CO2 hydrogenation to methanol over Cu-In intermetallic catalysts: effect of reduction temperature, J. Catal. 379 (2019) 78–89.
[33] L. Yao, X. Shen, Y. Pan, Z. Peng, Synergy between active sites of Cu-In-Zr-O catalyst in CO2 hydrogenation to methanol, J. Catal. 372 (2019) 74–85.
[34] M. Sadeghinia, M. Rezaei, A.N. Kharat, M.N. Jorabchi, B. Nematollahi, F. Zareiekordshouli, Effect of In2O3 on the structural properties and catalytic performance of the CuO/ZnO/Al2O3 catalyst in CO2 and CO hydrogenation to methanol, Mol. Catal. 484 (2020), 110776.
[35] B. Liang, J. Ma, X. Su, C. Yang, H. Duan, H. Zhou, S. Deng, L. Li, Y. Huang, Investigation on deactivation of Cu/Zno/Al2O3 catalyst for CO2 hydrogenation to methanol, Ind. Eng. Chem. Res. 58 (2019) 9030–9037.
[36] M. Behrens, I. Kasatkin, S. Kühl, G. Weinberg, Phase-pure Cu, Zn, Al hydrotalcite-like materials as precursors for copper rich Cu/ZnO/Al2O3 catalysts, Chem. Mater. 22 (2010) 386–397.
[37] R. Wang, Z. Yang, Synthesis and high cycle performance of Zn–Al–In-hydrotalcite as anode materials for Ni–Zn secondary batteries, RSC Adv. 3 (2013) 19924–19928.
[38] O. Krasnobaeva, I. Belomestnykh, V. Kogan, T. Nosova, V. Skorikov, T. Elizarova, V. Danilov, Indium-containing catalysts for oxidative dehydrogenation of organic compounds, Russ. J. Inorg. Chem. 59 (2014) 693–698.
[39] R. Wang, Z. Yang, B. Yang, T. Wang, Z. Chu, Superior cycle stability and high rate capability of Zn–Al–In-hydrotalcite as negative electrode materials for Ni–Zn secondary batteries, J. Power Sources 251 (2014) 344–350.
[40] M. Behrens, F. Girgsdies, A. Trunschke, R. Schlögl, Minerals as model compounds for Cu/ZnO catalyst precursors: structural and thermal properties and IR spectra of mineral and synthetic (zincian) malachite, rosasite and aurichalcite and a catalyst precursor mixture, Eur. J. Inorg. Chem. 2009 (2009) 1347–1357.
[41] P. Kowalik, M. Konkol, M. Kondracka, W. Próchniak, R. Bicki, P. Wiercioch, Memory effect of the CuZnAl-LDH derived catalyst precursor—In situ XRD studies, Appl. Catal. A: Gen. 464 (2013) 339–347.
[42] K. Ploner, L. Schlicker, A. Gili, A. Gurlo, A. Doran, L. Zhang, M. Armbrüster, D. Obendorf, J. Bernardi, B. Klötzer, Reactive metal-support interaction in the Cu-

In2O3 system: intermetallic compound formation and its consequences for CO2-selective methanol steam reforming, Sci. Technol. Adv. Mater. (2019) 356–366.
[43] A. Jedidi, S. Rasul, D. Masih, L. Cavallo, K. Takanabe, Generation of Cu–In alloy surfaces from CuInO 2 as selective catalytic sites for CO 2 electroreduction, J. Mater. Chem. A 3 (2015) 19085–19092.
[44] W. Jansen, J. Beckers, J. vd Heuvel, A.D. vd Gon, A. Bliek, H. Brongersma, Dynamic behavior of the surface structure of Cu/ZnO/SiO2 catalysts, J. Catal. 210 (2002) 229–236.
[45] M.C. Biesinger, L.W. Lau, A.R. Gerson, R.S.C. Smart, Resolving surface chemical states in XPS analysis of first row transition metals, oxides and hydroxides: Sc, Ti, V, Cu and Zn, Appl. Surf. Sci. 257 (2010) 887–898.
[46] M.C. Biesinger, Advanced analysis of copper X-ray photoelectron spectra, Surf. Interface Anal. 49 (2017) 1325–1334.
[47] P. Gao, F. Li, F. Xiao, N. Zhao, N. Sun, W. Wei, L. Zhong, Y. Sun, Preparation and activity of Cu/Zn/Al/Zr catalysts via hydrotalcite-containing precursors for methanol synthesis from CO 2 hydrogenation, Catal. Sci. Technol. 2 (2012) 1447–1454.
[48] F. Li, H. Zhan, N. Zhao, F. Xiao, Copper-based Perovskite Design and Its Performance in CO2 Hydrogenation to Methanol, Perovskite Materials-Synthesis, Characterisation, Properties, and Applications, IntechOpen, 2016.
[49] A. Yin, X. Guo, W.-L. Dai, K. Fan, The nature of active copper species in Cu-HMS catalyst for hydrogenation of dimethyl oxalate to ethylene glycol: new insights on the synergetic effect between Cu0 and Cu+, J. Phys. Chem. C 113 (2009) 11003–11013.
[50] J. Wu, S. Yang, Q. Liu, P. He, H. Tian, J. Ren, Z. Guan, T. Hu, B. Ni, C. Zhang, Cu Nanoparticles inlaid mesoporous carbon aerogels as a high performance desulfurizer, Environ. Sci. Technol. 50 (2016) 5370–5378.
[51] X. Zheng, H. Lin, J. Zheng, X. Duan, Y. Yuan, Lanthanum oxide-modified Cu/SiO2 as a high-performance catalyst for chemoselective hydrogenation of dimethyl oxalate to ethylene glycol, ACS Catal. 3 (2013) 2738–2749.
[52] S. Roso, C. Bittencourt, P. Umek, O. González, F. Güell, A. Urakawa, E. Llobet, Synthesis of single crystalline in 2 O 3 octahedra for the selective detection of NO 2 and H 2 at trace levels, J. Mater. Chem. C 4 (2016) 9418–9427.
[53] B. Pujilaksono, U. Klement, L. Nyborg, U. Jelvestam, S. Hill, D. Burgard, X-ray photoelectron spectroscopy studies of indium tin oxide nanocrystalline powder, Mater. Charact. 54 (2005) 1–7.
[54] P. Gao, F. Li, N. Zhao, F. Xiao, W. Wei, L. Zhong, Y. Sun, Influence of modifier (Mn, La, Ce, Zr and Y) on the performance of Cu/Zn/Al catalysts via hydrotalcite-like precursors for CO2 hydrogenation to methanol, Appl. Catal. A: Gen. 468 (2013) 442–452.
[55] C. Li, X. Yuan, K. Fujimoto, Development of highly stable catalyst for methanol synthesis from carbon dioxide, Appl. Catal. A: Gen. 469 (2014) 306–311.
[56] S. Kühl, J. Schumann, I. Kasatkin, M. Hävecker, R. Schlögl, M. Behrens, Ternary and quaternary Cr or Ga-containing ex-LDH catalysts—Influence of the additional oxides onto the microstructure and activity of Cu/ZnAl2O4 catalysts, Catal. Today 246 (2015) 92–100.
[57] S. Xiao, Y. Zhang, P. Gao, L. Zhong, X. Li, Z. Zhang, H. Wang, W. Wei, Y.J.C.T. Sun, Highly efficient Cu-based catalysts via hydrotalcite-like precursors for CO2 hydrogenation to methanol, Catal. Today 281 (2017) 327–336.
[58] S. Natesakhawat, J.W. Lekse, J.P. Baltrus, P.R. Ohodnicki Jr., B.H. Howard, X. Deng, C. Matranga, Active sites and structure–activity relationships of copper-based catalysts for carbon dioxide hydrogenation to methanol, ACS Catal. 2 (2012) 1667–1676.
[59] M. Zabilskiy, V.L. Sushkevich, D. Palagin, M.A. Newton, F. Krumeich, J.A.J.N. c. van Bokhoven, The unique interplay between copper and zinc during catalytic carbon dioxide hydrogenation to methanol, Nat. Commun. 11 (2020) 1–8.